COMPUTATIONALLY EFFICIENT TIME-VARYING ISAR IMAGING

Stephen R. Alty

King's College London, UK
Centre for Digital Signal Processing Research

Andreas Jakobsson

Dept. of Electrical Engineering
Karlstad University, Sweden

ABSTRACT

By exploiting the relative motion between the target and the radar, high-resolution images of moving targets can be produced using inverse synthetic aperture radar (ISAR). Recent studies have shown that accurate ISAR images can be obtained using the non-parametric high-resolution Capon and APES spectral estimators. In this paper, we propose a computationally efficient time-updating of the two-dimensional (2-D) Capon and APES spectral estimators using their inherent time-varying displacement structures. Numerical simulations indicate that the proposed implementation offers a significant reduction in computational complexity as compared to other recent implementations.

1. INTRODUCTION

Inverse synthetic aperture radar (ISAR) imaging offers the possibility to form high-resolution images of moving targets, and is an important technique to improve automatic target recognition performance. In conventional SAR, the imaged target is assumed stationary while the radar is moving. In ISAR, the radar is stationary (or moving) while the imaged target is moving in a noncooperative way, making ISAR imaging more difficult than SAR imaging [1]. Conventionally, ISAR images are formed using the Fourier transform, yielding estimates suffering from poor resolution and high sidelobes. More recent spectral estimation techniques have also been applied to SAR/ISAR imaging, with complex ISAR imaging recently attracting significant attention [2–6]. As shown in [7], maneuvering targets with nonuniform rotational motion will yield blurred images as a result of the time-varying Doppler-shifts corresponding to the cross-range of each scatterer. To mitigate this effect, computationally efficient time-varying implementations of the forward-only (F-O) Capon and APES spectral estimators were proposed in [5,6]. In [8], we proposed a 1-D time-updating of the block-based implementation of the forward-backward (FB) averaged Capon and APES algorithms proposed in [9]. Herein, we extend on this work, proposing a sliding-window time-updating of the 2-D Capon and APES spectral estimators as a way of forming time-varying ISAR imaging. The implementation is based on the estimators' inherent time-variant displacement structure, which allows for the time-updating of the inverse Cholesky factors of the (FB averaged) covariance matrix estimate using the numerically robust time-variant generalized Schur algorithm presented in [10]. The resulting time-updated spectral estimates offers a significant computational gain as compared with previously proposed approaches. Furthermore, via simulations, we found the suggested updating to be numerically superior, yielding a lower error propagation, as compared to a time-updated spectral estimate formed from the more direct (but computationally costlier) recursive updating of the sample covariance matrix proposed in [5, 6].

2. DATA MODEL

Following the notation in [3,6], let N denote the number of range samples and $\bar{N}$ the sliding window length along the cross-range dimension. Let $\{z_{n,t-\bar{n}}, n = 0, \ldots, N-1, \bar{n} = 0, \ldots, \bar{N}-1\}$ denote the phase history of a target of interest within the sliding window ending at index t in a cross-range. For a *generic* frequency pair $(\omega, \bar{\omega})$,

$$z_{n,t-\bar{n}} = \alpha_t(\omega, \bar{\omega}) e^{i\omega n + i\bar{\omega}(\bar{N}-1-\bar{n})} + v_{n,t-\bar{n}}(\omega, \bar{\omega}), \quad (1)$$

where $\alpha_t(\omega, \bar{\omega})$ and $v_{n,t-\bar{n}}(\omega, \bar{\omega})$ denote the time-varying complex amplitude of a 2-D cisoid, and an additive (colored) noise and interference term, respectively. We note that $\alpha_t(\omega, \bar{\omega})$ is assumed to be so slowly varying that it can be well modeled as being approximately stationary within the sliding window. Let the $(M \times \bar{M})$-tap matrices $\mathbf{H}_t(\omega, \bar{\omega})$ and $\mathbf{Z}_{l,t-\bar{l}}$ denote a 2-D finite impulse response (FIR) filter and the $(l, \bar{l})$th forward data (so-called "snapshot") matrix constructed from $z_{n,t-\bar{n}}$, respectively, and define (see [3,6] for a more detailed description of the structure of $\mathbf{H}_t(\omega, \bar{\omega})$ and $\mathbf{Z}_{l,t-\bar{l}}$)

$$\begin{aligned} \mathbf{h}_t(\omega, \bar{\omega}) &= \text{vec}\{\mathbf{H}_t(\omega, \bar{\omega})\} & (2) \\ \mathbf{z}_{l,t-\bar{l}} &= \text{vec}\{\mathbf{Z}_{l,t-\bar{l}}\} & (3) \end{aligned}$$

for $l = 0, \ldots, L-1, \bar{l} = 0, \ldots, \bar{L}-1$, where vec$(\cdot)$ denotes the operation consisting of stacking the columns of a matrix on top of each other, $L = N - M + 1$ and $\bar{L} = \bar{N} - \bar{M} + 1$. Let

$$\mathbf{R}_t = \sum_{l=0}^{L-1} \sum_{\bar{l}=0}^{\bar{L}-1} \mathbf{z}_{l,t-\bar{l}} \mathbf{z}_{l,t-\bar{l}}^* \tag{4}$$

denote the (forward) covariance matrix estimate, where $(\cdot)^*$ denotes the conjugate transpose. Furthermore, introduce

$$\mathbf{a}_{M,\bar{M}}(\omega, \bar{\omega}) = \mathbf{a}_M(\omega) \otimes \mathbf{a}_{\bar{M}}(\bar{\omega}), \tag{5}$$

with $\otimes$ denoting the Kronecker product,

$$\mathbf{a}_M(\omega) = \left[\begin{array}{cccc} 1 & e^{i\omega} & \ldots & e^{i\omega(M-1)} \end{array} \right]^T, \tag{6}$$

and $\mathbf{a}_{\bar{M}}(\bar{\omega})$ formed similar to $\mathbf{a}_M(\omega)$. The resulting (forward-only) Capon and APES estimates are formed as [3]

$$\hat{\alpha}_t(\omega, \bar{\omega}) = \frac{\mathbf{a}_{M,\bar{M}}^*(\omega, \bar{\omega}) \mathbf{Q}_t^{-1} \mathbf{Z}_t(\omega, \bar{\omega})}{L\bar{L}\mathbf{a}_{M,\bar{M}}^*(\omega, \bar{\omega}) \mathbf{Q}_t^{-1} \mathbf{a}_{M,\bar{M}}(\omega, \bar{\omega})}, \tag{7}$$

where $\mathbf{Q}_t^C = \mathbf{R}_t$ and $\mathbf{Q}_t^A = \mathbf{R}_t - \mathbf{Z}_t(\omega, \bar{\omega})\mathbf{Z}_t^*(\omega, \bar{\omega})/(L\bar{L})$, for the respective estimators, with

$$\mathbf{Z}_t(\omega, \bar{\omega}) = \sum_{l=0}^{L-1} \sum_{\bar{l}=0}^{\bar{L}-1} \mathbf{z}_{l,t-\bar{l}} e^{-il\omega - i\bar{\omega}(\bar{L}-1-\bar{l})}. \tag{8}$$

The FB averaged estimators, which often yield preferable performance, can be formed similarly [3]. In this paper, we propose a computationally efficient sliding window time update of the FB averaged estimates as an additional (column) vector in the *cross-range* direction becomes available.

3. PROPOSED RECURSIVE TIME-UPDATING

Using the matrix inversion lemma, one may evaluate the estimates in (7), and similarly their FB versions, using a number of matrix-vector multiplications and Fourier transforms of the inverse Cholesky factor of $\mathbf{R}_t$ [11]. This fact is exploited in the implementation presented in [9], which also uses the inherent displacement structure of $\mathbf{R}_t$ to efficiently evaluate the inverse Cholesky factors of $\mathbf{R}_t$ using the generalized Schur algorithm. In [8], we extended the 1-D version of this implementation by allowing for a time-updating using the time-variant generalized Schur algorithm [10]. Herein, we further extend on this work by allowing for the time-updating of 2-D data sets.

The time-variant FB covariance $M\bar{M} \times M\bar{M}$ matrix $\mathbf{R}_t$ is said to have a time-variant displacement structure if the matrix difference $\nabla\mathbf{R}_t$, defined by [10, 12]

$$\nabla\mathbf{R}_t = \mathbf{R}_t - \mathbf{F}_t \mathbf{R}_{t-\Delta} \mathbf{F}_t^*, \tag{9}$$

has low *rank*, say r, where $Lr \ll L\bar{L}$, for some lower triangular matrix $\mathbf{F}_t$. The time-variant displacement rank, r, provides a measure of the degree of structure present, with lower rank indicating stronger structure.

We note that a sliding window time-updating of the FB-version of $\mathbf{R}_t$ can be expressed as

$$\mathbf{R}_t = \mathbf{R}_{t-1} + \mathbf{G}_t \mathbf{J}_t \mathbf{G}_t^*, \tag{10}$$

where $\mathbf{G}_t$ and $\mathbf{J}_t$ are given below, allowing for a time-variant displacement structure with $\Delta = 1$ and $\mathbf{F}_t = \mathbf{I}$. Thus, $\nabla\mathbf{R}_t = \mathbf{G}_t\mathbf{J}_t\mathbf{G}_t^*$, where $\mathbf{G}_t$ is a $M\bar{M} \times Lr$ *generator* matrix and $\mathbf{J}_t$ is a $Lr \times \ Lr$ signature matrix with either $\pm\mathbf{I}_L$, where $\mathbf{I}_L$ denotes an $L \times L$ identity matrix, along its diagonal. Here,

$$\mathbf{J}_t = \left[\begin{array}{cccc} \mathbf{I}_L & 0 & 0 & 0 \\ 0 & \mathbf{I}_L & 0 & 0 \\ 0 & 0 & -\mathbf{I}_L & 0 \\ 0 & 0 & 0 & -\mathbf{I}_L \end{array} \right] \tag{11}$$

and

$$\mathbf{G}_t = \left[\begin{array}{cccc} \mathbf{X}_{l,t-\bar{l}} & \mathbf{J}_e\mathbf{X}_{l,t-\bar{l}}^* & \mathbf{Y}_{l,t-\bar{l}} & \mathbf{J}_e\mathbf{Y}_{l,t-\bar{l}}^* \end{array} \right]$$

where $\mathbf{J}_e$ denotes the exchange matrix, and with $\mathbf{X}_{l,t-\bar{l}}$ and $\mathbf{Y}_{l,t-\bar{l}}$ given by (12) and (13), found at the top of next page. From (11), we note that $r = 4$, typically[1] making Lr significantly less than $L\bar{L}$. We note that the positive-definite nature of $\mathbf{R}_t$ guarantees the existence of a unique (lower triangular) Cholesky factor, $\mathbf{L}_t$, such that

$$\mathbf{R}_t \triangleq \mathbf{L}_t\mathbf{L}_t^* = \left[\begin{array}{cc} \mathbf{L}_{t-1} & \mathbf{G}_t \end{array} \right] \left[\begin{array}{cc} \mathbf{I}_n & \mathbf{0} \\ \mathbf{0} & \mathbf{J}_t \end{array} \right] \left[\begin{array}{c} \mathbf{L}_{t-1}^* \\ \mathbf{G}_t^* \end{array} \right]$$

The above relation can be extended to allow for the direct evaluation of the time-updated *inverse* Cholesky factors $\mathbf{U}_t$, where $\mathbf{R}_t^{-1} = \mathbf{U}_t\mathbf{U}_t^*$, i.e.,

$$\begin{aligned} \left[\begin{array}{cc} \mathbf{R}_t & \mathbf{I} \\ \mathbf{I} & \mathbf{R}_t^{-1} \end{array} \right] &= \left[\begin{array}{cc} \mathbf{L}_{t-1} & \mathbf{G}_t \\ \mathbf{U}_{t-1} & \mathbf{0} \end{array} \right] \\ &\times \left[\begin{array}{cc} \mathbf{I}_n & \mathbf{0} \\ \mathbf{0} & \mathbf{J}_t \end{array} \right] \left[\begin{array}{cc} \mathbf{L}_{t-1}^* & \mathbf{U}_{t-1}^* \\ \mathbf{G}_t^* & \mathbf{0} \end{array} \right] \end{aligned} \tag{14}$$

Hence, it follows that there exists an $[\mathbf{I}_n \oplus \mathbf{J}_t]$-unitary *rotation* matrix[2], $\mathbf{\Gamma}_t$, such that

$$\left[\begin{array}{cc} \mathbf{L}_t & \mathbf{0} \\ \mathbf{U}_t & \mathbf{H}_t^* \end{array} \right] = \left[\begin{array}{cc} \mathbf{L}_{t-1} & \mathbf{G}_t \\ \mathbf{U}_{t-1} & \mathbf{0} \end{array} \right] \mathbf{\Gamma}_t \tag{15}$$

Note that $\mathbf{\Gamma}_t$ has the effect of rotating the generator matrix onto the expression $\mathbf{L}_{t-1}$ and $\mathbf{U}_{t-1}$ to produce the updated Cholesky factor $\mathbf{L}_t$ and inverse Cholesky factor $\mathbf{U}_t$, respectively. We note that a block zero entry in the left-hand side

[1] Depending on the application, $L\bar{L}$ is usually very large.

[2] Here, a $\mathbf{J}$-unitary matrix $\mathbf{\Theta}$ is defined as any matrix $\mathbf{\Theta}$ such that $\mathbf{\Theta}\mathbf{J}\mathbf{\Theta}^* = \mathbf{J}$. Further, $\mathbf{a} \oplus \mathbf{b}$ denotes a matrix with the sub-matrices $\mathbf{a}$ $\{n \times n\}$ and $\mathbf{b}$ $\{m \times m\}$ concatenated to produce a matrix of size $\{(m+n) \times (m+n)\}$.

$$\mathbf{X}_{l,t-\bar{l}} = \left[\begin{array}{cccc} \mathbf{z}_{l,t+(l-1)\bar{l}-l+1} & \mathbf{z}_{l,t+(l-1)\bar{l}-l+2} & \cdots & \mathbf{z}_{l,t+(l-1)\bar{l}} \end{array} \right] \tag{12}$$

$$\mathbf{Y}_{l,t-\bar{l}} = \left[\begin{array}{cccc} \mathbf{z}_{l,t-\bar{l}+1} & \mathbf{z}_{l,t-\bar{l}+2} & \cdots & \mathbf{z}_{l,t-\bar{l}+l} \end{array} \right] \tag{13}$$

of (15) and the inverse generator matrix $\mathbf{H}_t^*$ are also produced as a result. The rotational transform $\mathbf{\Gamma}_t$ is typically implemented as a sequence of elementary transforms, such that $\mathbf{\Gamma}_t = \mathbf{\Gamma}_t^1\mathbf{\Gamma}_t^2 \cdots \mathbf{\Gamma}_t^L$, where $\mathbf{\Gamma}_t^k$ annihilates the kth row of the generator matrix (and simultaneously generates the kth row of the inverse generator matrix). The rotation matrices $\mathbf{\Gamma}_t$ can be formed in numerous different ways. They are, however, typically formed from a combination of the *Householder* and *Givens* rotations. Both of these transforms have the general form

$$\left[\begin{array}{cc} a & b \end{array} \right] \mathbf{\Theta} = \left[\begin{array}{cc} \alpha & 0 \end{array} \right], \tag{16}$$

where $\alpha_H = \sqrt{|a|^2 - |b|^2}$ for a Householder and $\alpha_G = \sqrt{|a|^2 + |b|^2}$ for a Givens rotation. The corresponding rotation matrices are given as

$$\mathbf{\Theta}_H = \frac{1}{\sqrt{|a|^2 - |b|^2}} \left[\begin{array}{cc} a & -b \\ -b^* & a \end{array} \right] \tag{17}$$

and

$$\mathbf{\Theta}_G = \frac{1}{\sqrt{|a|^2 + |b|^2}} \left[\begin{array}{cc} a & b \\ b^* & -a \end{array} \right] \tag{18}$$

The Givens rotation is used for "*updating*" the factor with new samples and the Householder rotation has the effect of "*downdating*" the factor by removing those samples which are no longer present in the time-updated sample frame. In this way, an appropriate combination of rotations can be determined to correctly time-update each Cholesky factor column vector in turn. One should note that in practice each column of the Cholesky factor (and inverse) is concatenated with the generator matrix to make an $\{M\bar{M}+1\} \times \{Lr+1\}$ matrix, as illustrated in (19), and as each vector is updated, this process is repeated whilst each row of the generator matrix is annihilated until all the column vectors of the new Cholesky (and inverse) factors are produced.

$$\left[\begin{array}{ccc} l & g & g \\ l & g & g \\ l & g & g \\ u & 0 & 0 \end{array} \right] \xrightarrow{\mathbf{\Gamma}_t^1} \left[\begin{array}{ccc} l' & 0 & 0 \\ l' & g' & g' \\ l' & g' & g' \\ u' & h & h \end{array} \right] \text{ followed by}$$
$$\left[\begin{array}{ccc} l & g' & g' \\ l & g' & g' \\ u & h' & h' \\ u & 0 & 0 \end{array} \right] \xrightarrow{\mathbf{\Gamma}_t^2} \left[\begin{array}{ccc} l' & 0 & 0 \\ l' & g'' & g'' \\ u' & h'' & h'' \\ u' & h' & h' \end{array} \right] \text{ etc.} \tag{19}$$

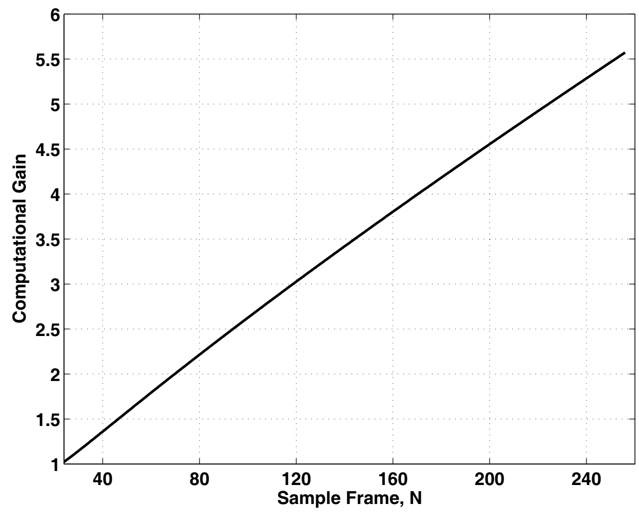

Fig. 1. Computational gain of evaluating the amplitude spectrum Capon estimate using the proposed method as compared with the method in [6].

4. NUMERICAL EXAMPLES

To the best of our knowledge, the currently most efficient way to evaluate the 2-D Capon and APES spectral estimates is the method introduced in [6]. There, it was found that the complexity of evaluating the amplitude spectrum Capon estimate is $\mathcal{O}(4M^2L^3 + 10M^4L + 5LK^2 log_2 K)$ operations per iteration. The herein proposed method requires $\mathcal{O}(2N^2 log_2 N^2 + M^2(4L + 12M^2 log_2 M^2 + 2N^2 log_2 N^2) + 4M^2 log_2 M^2 + N^2 log_2 N^2 + 2K^2 log_2 K^2)$ operations per iteration. For simplicity, we here assume that $N = \bar{N}$, $M = \bar{M} = N/2$, and $K = \bar{K} = 2N$, where K denotes the number of grid points to be evaluated in the image. Figure 1 illustrates the computational gain of evaluating the amplitude spectrum Capon using the proposed algorithm as compared to the method presented in [6]. As seen from the figure, the presented method offers a significant computational gain[3] even for modest data sizes such as $N > 32$. Furthermore, we have noted that the proposed method offers a significant improvement in error propagation as compared to the method in [6]. The latter requires two matrix inversions per iteration, whereas the formed relies on Givens and Householder rotations to form the updating. In our

[3]Similar complexity gain is achieved for the APES spectral estimate.

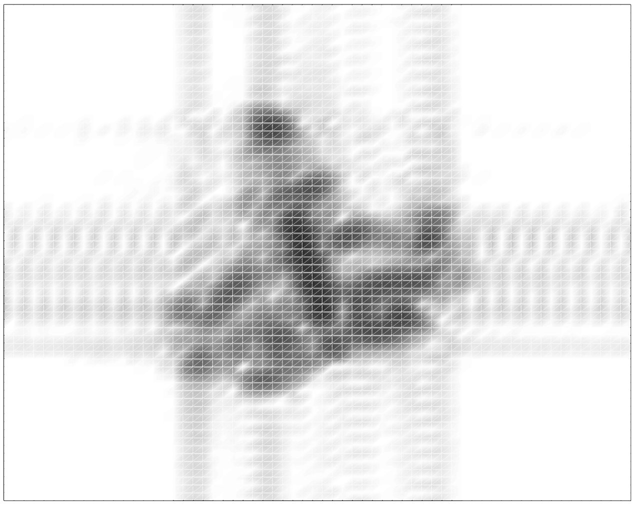

Fig. 2. An example of an ISAR image of a simulated moving MIG-25 airplane obtained using the windowed FFT.

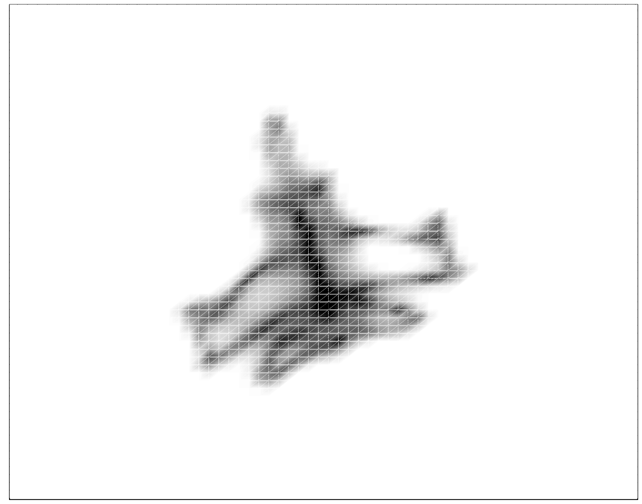

Fig. 3. An example of an ISAR image of a simulated moving MIG-25 airplane obtained using the Capon estimate.

experience, these rotations are numerically robust, yielding a preferable error propagation [8]. Finally, Figures 2 and 3 illustrate the quality improvement in the ISAR image offered by the Capon approach as compared to a traditional Fourier-based technique. The images are formed from $N = \bar{N} = 32$ signal phase history data of a simulated fast rotating MIG-25 airplane, evaluated on $K = \bar{K} = 2N$ grid points. Figure 2 shows the ISAR image obtained by applying the windowed 2-D fast Fourier transform (FFT) method, whereas Figure 3 shows the corresponding power spectral Capon image. As can be seen in the figures, the Capon estimate offers a significantly clearer image of the airplane as compared to the FFT-based image (see also [5,6] for further examples of achieved quality improvements using the different estimators). In conclusion, we note that further complexity reductions are expected by also allowing for recursive updating of the filter polynomials, and we are currently extending the presented work in this direction.

5. ACKNOWLEDGEMENT

The authors are grateful to Prof. J. Li of the University of Florida, Gainesville, for kindly supplying the simulated MiG-25 airplane data.

6. REFERENCES

[1] C. V. Jakowatz, Jr., D. E. Wahl, P. H. Eichel, D. C. Ghiglia, and P. A. Thomson, *Spotlight-Mode Synthetic Aperture Radar: A Signal Processing Approach*, Kluwer, Norwell, M.A., 1996.

[2] A. W. Rihaczek and S. J. Hershkowitz, *Radar Resolution and Complex-Image Analysis*, Artech House, Norwood, M.A., 1996.

[3] J. Li and P. Stoica, “Adaptive Filtering Approach to Spectral Estimation and SAR Imaging,” *IEEE Trans. Signal Processing*, vol. 44, no. 6, pp. 1469–1484, June 1996.

[4] S. R. DeGraaf, “SAR Imaging via Modern 2-D Spectral Estimation Methods,” *IEEE Trans. Image Processing*, vol. 7, no. 5, pp. 729–761, May 1998.

[5] R. Wu, Z.-S. Liu, and J. Li, “Time-varying complex spectral analysis via recursive APES,” *IEE Proc. Radar, Sonar and Navigation*, vol. 145, pp. 354–360, December 1998.

[6] Z.-S. Liu, R. Wu, and J. Li, “Complex ISAR Imaging of Maneuvering Targets via the Capon Estimator,” *IEEE Trans. Signal Processing*, vol. 47, no. 5, pp. 1262–1271, May 1999.

[7] V. C. Chen, “Time-Frequency based ISAR Image Formation Technique,” in *Proc. SPIE: Algorithms Synthetic Aperture Radar Imagery IV*, April 1997, pp. 43–54.

[8] S. R. Alty, A. Jakobsson, and E. G. Larsson, “Efficient Time-Recursive Implementation of Matched Filterbank Spectral Estimators,” *IEEE Trans. on Circuits and Systems I: Regular Papers*, vol. 52, no. 3, March 2005.

[9] E. G. Larsson and P. Stoica, “Fast Implementation of Two-Dimensional APES and Capon Spectral Estimators,” *Multidimensional Systems and Signal Processing*, vol. 13, no. 1, pp. 35–54, Jan. 2002.

[10] A. H. Sayed, H. Lev-Ari, and T. Kailath, “Time-variant Displacement Structure and Triangular Arrays,” *IEEE Trans. Signal Processing*, vol. 42, pp. 1052–1062, May 1994.

[11] P. Stoica, A. Jakobsson, and J. Li, “Matched-Filterbank Interpretation of Some Spectral Estimators,” *Signal Processing*, vol. 66, no. 1, pp. 45–59, April 1998.

[12] T. Kailath and A. H. Sayed, *Fast Reliable Algorithms for Matrices with Structure*, SIAM, Philadelphia, USA, 1999.